34th Annual International Conference of the IEEE EMBS
San Diego, California USA, 28 August - 1 September, 2012

Towards a Noise Prediction Model for *In Vivo* Neural Recording

Carolina Mora López, Marleen Welkenhuysen, Silke Musa, Wolfgang Eberle, Carmen Bartic[†], Robert Puers[♣], Georges Gielen[♣]
Imec, Leuven, Belgium
[†]Department of Physics and Astronomy, KU Leuven, Leuven, Belgium
[♣]Electrical Engineering Department-ESAT, KU Leuven, Leuven, Belgium
E-mail: Carolina.MoraLopez@imec.be

Abstract— **The signal-to-noise ratio of *in vivo* extracellular neural recordings with microelectrodes is influenced by many factors including the impedance of the electrode-tissue interface, the noise of the recording equipment and biological background noise from distant neurons. In this work we study the different noise sources affecting the quality of neural signals. We propose a simplified noise model as an analytical tool to predict the noise of an electrode given its geometrical dimensions and impedance characteristics. With this tool we are able to quantify different noise sources, which is important to determine realistic noise specifications for the design of electronic neural recording interfaces.**

I. Introduction

Considerable technological advances in the field of *in vivo* neural implants (probes) have given rise to a new generation of devices with high-density electrode arrays for large-scale recording of extracellular neural signals [1]. Despite such progress, the initially high performance of these devices often deteriorates during chronic *in vivo* applications [2]. The signal quality, expressed as the signal-to-noise ratio (SNR), and the long-term recording stability are related to multiple factors including: (i) the electrode-neuron distance [3], (ii) the electrode surface area [4], [5], (iii) the electrode-tissue interface impedance [5], [6], (iv) the extent of the insertion trauma (i.e. edema) and foreign body response (i.e. encapsulation) [2], [4], and (v) the bandwidth used in the recording system [5].

It has been shown that the thermal noise generated by an electrode-tissue interface is proportional to its impedance [5], [6], [7]. This impedance is mainly determined by the material characteristics and the electrode surface area. As the impedance scales inversely with the electrode area, small electrodes with higher impedance should generate higher noise. High-impedance electrodes will also be more prone to noise/signal coupling from other sources and signal loss through shunt pathways. In chronically implanted electrodes, the electrode-tissue interface noise is also affected by local changes in the surrounding tissue (due to the foreign body response). The formation of a low-conductivity encapsulation tissue around the electrodes increases the impedance and the noise of the interface over time and can lead to the inability to record action potentials [2].

Electronic data acquisition systems can provide integrated amplification and filtering of the neural signals before they are further processed. The bandwidth of the filters can be properly selected to reject low- and high-frequency noise bands thus reducing the overall noise. On the other hand, electronic circuits themselves generate noise that adds up to the total recording noise. The contribution of this electronic noise can be significant or insignificant depending on the strength of the other noise sources.

The goal of this study is to model and quantify the different noise sources that affect *in vivo* extracellular recording of neural activity. The simplified noise model described here provides an analytical tool to predict the total noise of an electrode given its geometrical dimensions and empirically determined impedance characteristics. This tool is particularly useful to determine noise specifications for the design of electronic neural recording interfaces. In this study, the noise of Pt and TiN electrodes of different sizes has been predicted and measured *in vitro* (phosphate buffered saline (PBS)) and *in vivo* (anaesthetized rats). We have focused on the frequency band of the action potential signals (i.e. 300-6000 Hz), where the noise constraints are more severe. The results show a good agreement between the experimental data and the predicted values derived from the given noise models.

II. Materials and Methods

A. Electrode-Tissue Interface Noise Modelling

The overall noise of an electrode-tissue interface has contributions from different sources: (i) the tissue/bulk thermal noise, (ii) the electrode-electrolyte interface noise, (iii) the electronic noise, (iv) the biological noise and (v) other coupled external noise sources. The latter can greatly be reduced by proper grounding and shielding techniques. The other four sources have been included in the analytical model depicted in Fig. 1. Tissue noise is modelled as the thermal noise generated by the solution/spreading or tissue/encapsulation resistance (R_b in Fig. 1). For flat disc electrodes, it can be expressed as [6], [8]

$$\overline{V}^2_{n-tissue} = 4kTR_b\Delta f \approx kT\frac{\rho_{tissue}}{r_s}\Delta f\,, \qquad (1)$$

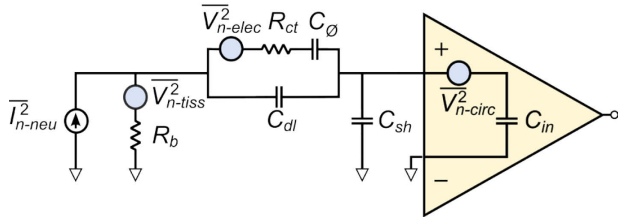

Fig. 1. Noise model for *in vivo* neural recording with microelectrodes.

where k is the Boltzman constant, T is the temperature, R_b is the bulk resistance, ρ_{tissue} is the tissue/electrolyte resistivity, r_s is the radius of the electrode and $\Delta f = f_2 - f_1$ is the bandwidth of the measurement, with f_2 being the upper corner and f_1 the lower corner of the filter. In our *in vitro* noise predictions, ρ_{tissue} corresponds to the PBS resistivity. For the *in vivo* noise calculations, literature-reported values of tissue resistivity (i.e. 300 Ω·cm) were used [4]. Higher values can be used to account for tissue encapsulation effects during chronic experiments.

The impedance of the electrode was modelled as a charge transfer resistor (R_{ct}) in parallel with the double-layer capacitor (C_{dl}). A pseudocapacitor (C_{ϕ}) in series with R_{ct} accounted for the capacitive behaviour of faradaic electrode processes [10]. The electrode noise is then the thermal noise generated by the resistor R_{ct}, low-pass filtered by the natural filter formed by R_{ct} and C_{dl} [9]. Assuming that the shunt capacitance (C_{sh}) of the electrode and the input capacitance (C_{in}) of the amplifier are sufficiently small, producing negligible signal loss, the electrode noise can be expressed as [6], [9]

$$\overline{V}^2_{n-elec} = \frac{2kT\alpha}{\pi C_{dl}} \tan^{-1} 2\pi R_{ct} C_{dl} \alpha f \Big|_{f=f1}^{f=f2}, \qquad (2)$$

where $\alpha = C_{\phi}/(C_{\phi} + C_{dl})$. For the noise estimations, values for R_{ct}, C_{dl}, C_{ϕ} (only used for TiN electrodes) and C_{sh} were extracted from measured electrode impedances fitted to the equivalent circuit shown in Fig. 1, similar to [10] (data not shown). C_{in} was taken from the recording circuit specifications.

The noise of the recording electronic circuits ($\overline{V}^2_{n-circ}$) is mainly determined by the thermal and flicker noise generated by the input amplifier [9]. The total electronic noise in the frequency band of interest (Δf) is usually specified as the input-referred noise of the recording system and is normally expressed as a root-mean-square (rms) value.

Simulations have indicated that the biological noise, $\overline{V}^2_{n-neu}$, generated by the spiking activity of distant neurons may be one of the major noise sources [5]. In our model it is represented by the current source $\overline{I}^2_{n-neu}$. Another study suggested that this noise exhibits a $1/f^x$ frequency dependence [6], where x depends on several experimental conditions and can vary between 0.68 and 1.38 [11]. In our noise estimations, this source was not taken into account, but rather we extracted it from our *in vivo* measurements.

For *in vitro* or *in vivo* recordings, the total noise at the input of the recording amplifier is given by

$$\overline{V}^2_{n-total} = \overline{V}^2_{n-tissue} + \overline{V}^2_{n-elec} + \overline{V}^2_{n-circ} + \overline{V}^2_{n-neu}. \qquad (3)$$

For small electrodes that exhibit very high impedances, C_{sh} and C_{in} will start to play an important role as signal and noise attenuators due to the voltage divider formed at the input of the amplifier. Thus, all the noise sources, except $\overline{V}^2_{n-circ}$, are attenuated by a factor β^2 given by

$$\beta^2 = \left| 1 + \frac{Z_{elec}}{Z_{in} \parallel Z_{sh}} \right|^2, \qquad (4)$$

where Z_{elec} is the total impedance of the electrode, Z_{in} is the input impedance of the amplifier and Z_{sh} is the shunt impedance (all impedance values were calculated at 1 kHz).

B. Electrode Impedance Measurements

Electrochemical impedance spectroscopy (EIS) was performed in PBS (0.150M NaCl, 0.016M Na_2HPO_4, 0.004M KH_2PO_4, pH 7.4). All chemicals were analytical grade and used as delivered (Sigma-Aldrich, USA). Experiments were conducted in a glass beaker using a three-electrode configuration placed inside a Faraday cage. A commercial Ag/AgCl (3M KCl) reference electrode (Radiometer Analytical, France) was used together with a large-area Pt counter electrode. A 10 mV_{rms} AC signal was applied between 1 Hz and 100 kHz using an Autolab PSTAT302N potentiostat with integrated frequency response analyzer controlled by the NOVA software (version 1.8, Ecochemie, Netherlands). We used OriginPro 8.1 (OriginLab, USA) and ZView (Scribner, USA) for the data analysis and the nonlinear least-square fitting of the EIS spectra, respectively.

C. In Vitro Noise Measurement

In order to measure the electrode-electrolyte noise *in vitro*, we packaged in-house fabricated multi-electrode test chips with different electrode diameters (5, 10, 25 or 50 µm) and materials (Pt or TiN) on custom printed circuit boards (PCBs). A glass ring was glued on top of the PCBs to contain PBS with a resistivity of 62.5Ω·cm. The noise from each electrode was measured against a Ag/AgCl reference electrode. The *in vitro* experimental setup consisted of a mechanical holder with electrical contacts to the test chip and a PCB containing custom electronic circuits for amplification and filtering of the signals [12]. The noise of the recording electronic system was 1.46 μV_{rms}. All measurements were performed at 22 ºC inside a Faraday cage to minimize noise coupling from external sources.

Noise measurements were performed using a gain of 1000 V/V and a fourth-order band-pass filter from 300 Hz to 6 kHz. The total measured input-referred noise contained (i) the intrinsic noise of the input amplifier ($\overline{V}^2_{n-circ}$) and (ii) the intrinsic noise of the electrode-electrolyte interface ($\overline{V}^2_{n-elec}$ + $\overline{V}^2_{n-tissue}$). The rms noise was calculated as the standard deviation of the data set.

D. In Vivo Noise Measurement

A similar setup was used for noise and brain activity measurements *in vivo*. Here we used in-house fabricated implantable micro-machined neural probes [13] of 1 cm

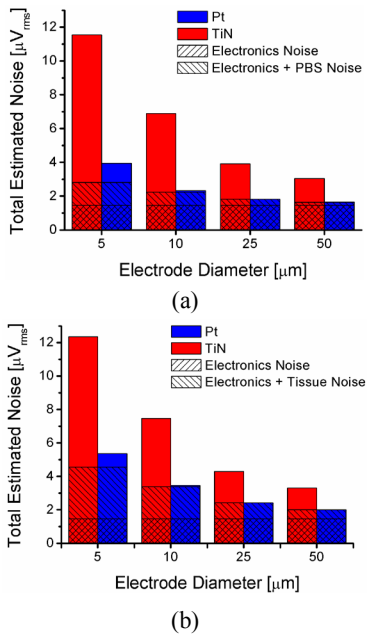

Fig. 2. Estimated noise for different electrode sizes and materials. (a) *In vitro* noise estimation at 22 ºC. (b) *In vivo* noise estimation at 37 ºC.

length, containing electrodes of different materials (Pt or TiN) and diameters (25 or 50 µm). These electrodes were fabricated using the same process (i.e. lift-off of sputtered 200-nm-thick Pt or 100-nm-thick TiN films) as the *in vitro* electrodes, thus they are directly comparable. The neural probes were connected by means of a short flat cable to the custom PCB with the recording electronic circuit [12]. The insertion setup was shielded with a Faraday cage during experiments.

All *in vivo* measurements were performed in anaesthetized rats using the same settings as for the *in vitro* measurements, i.e. 1000 V/V and 300 Hz-6 kHz band-pass filter. In order to identify the magnitude of the unknown biological background noise, we performed measurements before and after injecting a euthanizing drug. Thus, the total input-referred noise measured before the injection contained (i) the intrinsic noise of the input amplifier ($\overline{V}^2_{n-circ}$), (ii) the intrinsic noise of the electrode-tissue interface ($\overline{V}^2_{n-elec}$ + $\overline{V}^2_{n-tissue}$), and (iii) the biological noise ($\overline{V}^2_{n-neu}$). After animal death, the biological noise is absent. In order to minimize the artificial contribution of recorded spikes to the calculated noise, we extracted the *in vivo* rms noise using the median of the data set as described in [14].

E. Animal Surgery

All *in vivo* experiments were carried out in accordance to the protocols approved by the ethical committee of the KU Leuven, Belgium and with the legal requirements of our national authority. The rats (n=8) were placed under general anaesthesia by chloral hydrate (0.5 g/kg rat s.c.) and standard surgery protocols were applied [15]. Neural implants were inserted into the hippocampus (coordinates: 3.6 mm posterior of bregma, 2.4 mm lateral to the midline and 2.9 to 3.7 mm ventral of the dura mater [16]) at a constant speed of 10 µm/s using an electronically controlled hydraulic micro-drive (D. Kopf Instruments). Once all contacts of the probe were in the

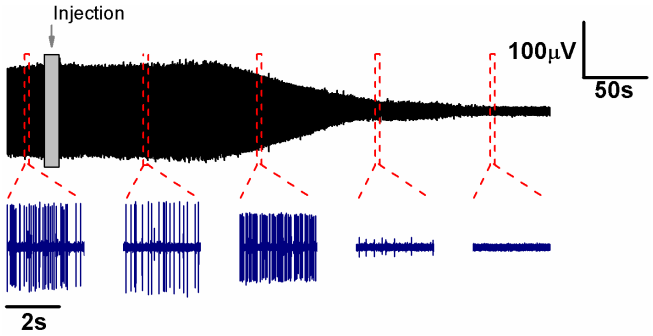

Fig. 3. 7 minutes recording of *in vivo* noise and neural spikes (gain: 1000 V/V, bandwidth: 300-6000 Hz). Measurements were obtained with a 25µm-diameter Pt electrode positioned in the hippocampus. The background activity decay was monitored after drug injection until the time of death. Noise was calculated before (with significant neural activity) and after euthanasia in order to identify the different noise sources.

hippocampus and neuronal activity was seen on one or more contacts, insertion was stopped and a baseline recording was acquired. Next, the rat was euthanized with an overdose of pentobarbital (Nembutal, 3ml i.p.) and the breathing and heart rate was monitored throughout the recording. The recording was stopped 5 min after the time of death.

III. Results And Discussion

In vitro and *in vivo* noise estimations (at 22 ºC and 37 ºC respectively) for the different electrode sizes and materials were done following the analysis in Section IIA. In Fig. 2 we compare the estimated *in vitro* and *in vivo* noise for Pt and TiN electrodes of different sizes. As expected, the noise is higher for smaller electrodes as they have higher impedances. For the 50 and 25 µm diameter Pt electrodes, the total noise is dominated by the electronic and electrolyte noises, while the electrode noise only starts to play a role for smaller sizes. Thus, electronic noise becomes relatively less important for small Pt electrodes which can relax the design specifications of integrated recording circuits. In contrast, noise in TiN electrodes is always dominated by the electrode noise, making the other noise sources negligible. The estimated *in vivo* noise is higher due to the higher resistivity of the tissue (compared to PBS) and the higher temperature (i.e. due to the thermal noise).

Fig. 3 shows a 7-minute extract of an *in vivo* neural recording performed with a 25 µm diameter Pt electrode. Similar results were obtained for all electrode sizes and materials. In all cases, neural activity persisted for a few minutes after drug injection, followed by a gradual decrease in amplitude or a diminished firing rate until the neural activity completely ceased (minimum 5 minutes after injection). After brain death, a noticeable increase in the noise level was observed (data not shown) attributed to an increased brain impedance [17]. Noise measurements were done just before this effect occurred. Fig. 4 shows the rms noise measured before and after euthanasia for the different contacts. The error bars represent one standard deviation of the data. By subtracting the two noise (power) measurements, the biological noise ($\overline{V}^2_{n-neu}$) was found to be 0.94 ± 0.3 and 1.43 ± 0.56 µVrms for Pt (50 and 25 µm, respectively), and 0.99 ± 0.35 and 1.06 ± 0.32 µVrms for TiN (50 and 25 µm, respectively).

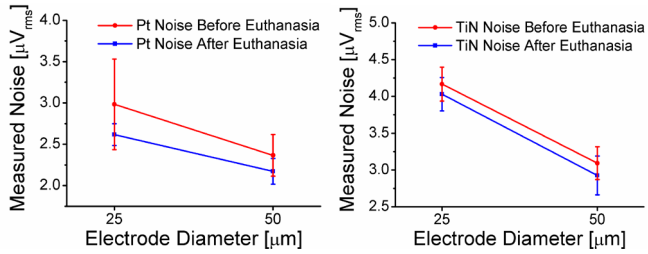

(a) (b)

Fig. 4. *In vivo* noise measurements before and after euthanasia for different electrode sizes and materials. The error bars represent one standard deviation of the data. Measurements before and after euthanasia were significantly different ($P < 0.05$) according to Mann-Whitney U-test. (a) Pt noise. (b) TiN noise.

Fig. 5 finally compares the measured and estimated noises for both *in vitro* and *in vivo* (without biological noise). The estimates were in very good agreement with the experimental data.

CONCLUSIONS

In this study we presented a simplified analytical model for noise prediction during *in vivo* neural recording. *In vitro* and *in vivo* noise measurements validated the presented noise model and demonstrated the feasibility of predicting the total noise of an electrode given its geometrical dimensions and impedance characteristics. The usability of this model is based on two assumptions: (i) the input impedance and noise specifications of the electronic acquisition system are well known or their effect can be ignored, and (ii) the electrode-tissue impedance can be fitted to a simple equivalent circuit. Electrodes with more complex electrochemical properties may require additional circuit elements in order to get accurate fittings. In that case, more elaborated expressions for the electrode noise must be derived. Tissue resistivity changes due to edema or encapsulation formed during chronic implantations will also affect the correctness of the predicted noise.

ACKNOWLEDGMENTS

This work was funded in part by the Flemish Government (IWT SBO grant BrainStar). The authors thank Alexandru Andrei for the design of the neural probes and Dimiter Prodanov for helping with the *in vivo* setup.

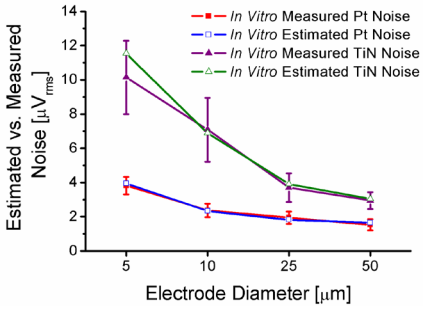

(a)

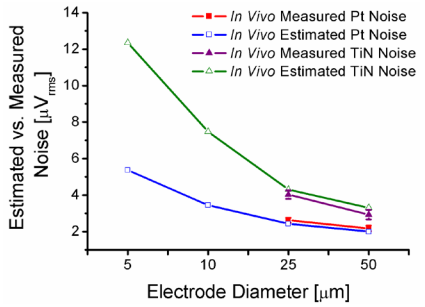

(b)

Fig. 5. Estimated vs. measured noise for different electrode sizes and materials. *In vivo* noise was measured with only 2 electrode sizes, i.e. 50 and 25 μm diameter. The error bars represent one standard deviation of the data. (a) *In vitro* noise. (b) *In vivo* noise.

REFERENCES

[1] Kevin Otto, Kip A. Ludwig, Daryl R. Kipke, "Acquiring brain signals from within the brain," in *Brain-Computer Interfaces: Principles and Practice,* Jonathan R. Wolpaw and Elizabeth Winter Wolpaw, Eds. New York: Oxford University Press, 2012.

[2] V. S. Polikov, P. A. Tresco, and W. M. Reichert, "Response of brain tissue to chronically implanted neural electrodes," *J. Neurosci. Meth.*, vol. 148, pp. 1–18, 2005.

[3] D. R. Humphrey and E. M. Schmidt, "Extracellular single-unit recording methods," in *Neurophysiological Techniques: Applications to Neural Systems*, A. A. Boulton, Ed. Totowa, NJ: Humana, 1990.

[4] M.A. Moffitt and C.C. McIntyre, "Model-based analysis of cortical recording with silicon microelectrodes," *Clin. Neurophysiol.*, vol. 116, no. 9, pp. 2240-2250, Sep. 2005.

[5] S. F. Lempka, M. D. Johnson, M. A. Moffitt, K. J. Otto, D. R. Kipke, and C. C. McIntyre, "Theoretical analysis of intracortical microelectrode recordings," *J. Neural Eng.*, vol. 8, p. 045006, 2011.

[6] Z. Yang, Q. Zhao, E. Keefer and W. Liu, "Noise Characterization, Modeling, and Reduction for In Vivo Neural Recording," *Advances in Neural Information Processing Systems*, pp 2160-2168, 2010.

[7] A. Hassibi et al., "Comprehensive study of noise processes in electrode–electrolyte interfaces," *J. Appl. Phys.*, vol. 96, no. 2, pp. 1074–1082, Jul. 2004.

[8] West,A.C. and J. Newman, "Current Distributions on Recessed Electrodes", *Jour. of the Electrochemical Soc.*, Vol. 138, No. 6, 1991.

[9] B. Razavi, *Design of Analog CMOS Integrated Circuits*. Boston, MA: McGraw-Hill, 2001.

[10] Musa, S. *Design, fabrication and characterization of a neural probe for deep brain stimulation and recording.* PhD Thesis, KU Leuven, 2011.

[11] J. Davidsen and H. G. Schuster, " Simple model for 1/f$^{\alpha}$ noise", *Phys. Rev. E*, 65, pp. 026120-1-4, 2002.

[12] Mora Lopez, C.; Prodanov, D.; Braeken, D.; Gligorijevic, I.; Eberle, W.; Bartic, C.; Puers, R.; Gielen, G.; , "A Multichannel Integrated Circuit for Electrical Recording of Neural Activity, With Independent Channel Programmability," *Biomedical Circuits and Systems, IEEE Transactions on* , vol.PP, no.99, pp.1, 0.

[13] Musa, S.; Welkenhuysen, M.; Huys, R.; Eberle, W. and Bartic, C., "Planar 2D-array neural probe for deep brain stimulation and recording (DBSR)". *Proc. of the 4th Euro. Cong. of the Intern.Feder. for Med. and Bio. Eng.- MBEC.,* vol. 22, pp. 2421-2425, Nov.2008.

[14] R. Q. Quiroga, Z. Nadasdy, and Y. Ben-Shaul, "Unsupervised spike detection and sorting with wavelets and superparamagnetic clustering," *Neural Computation*, vol. 16, no. 8, pp. 1661–1687, 2004.

[15] Welkenhuysen, M.; Andrei, A.; Ameye, L.; Eberle, W.; Nuttin, B.; , "Effect of Insertion Speed on Tissue Response and Insertion Mechanics of a Chronically Implanted Silicon-Based Neural Probe," *Biomed. Eng., IEEE Transactions on* , vol.58, no.11, pp.3250-3259, Nov. 2011.

[16] G. Paxinos and C.Watson, *The Rat Brain in Stereotactic Coordinates*, 2nd ed. Sydney: Academic, 2005.

[17] H. Gamba and D. Delpy, "Measurement of electrical current density distribution within the tissues of the head by magnetic resonance imaging," *Med. Biol. Eng. Comput.*, vol. 36, no. 2, pp. 165–170, 1998.